KIT in oocytes: a key factor for oocyte survival and reproductive lifespan

Yi Luan,[a,c] Wonmi So,[a,c] Rosemary Dong,[a] Amirhossein Abazarikia,[a] and So-Youn Kim[a,b,*]

[a]Olson Centre for Women's Health, Department of Obstetrics and Gynaecology, College of Medicine, University of Nebraska Medical Centre, Omaha, NE, USA
[b]Fred and Pamela Buffett Cancer Centre, University of Nebraska Medical Centre, Omaha, NE, USA

eBioMedicine
2024;106: 105263
Published Online xxx
https://doi.org/10.1016/j.ebiom.2024.105263

Summary

Background The KITL-KIT interaction is known as an important initiator in oocyte activation through the downstream pathway of PI3K-AKT-FOXO3 signalling. Previous studies utilising germ cell-specific *Kit* mutant knockin and kinase domain knockout models with *Vasa-Cre* suggested the crucial role of KIT in oocyte activation at the primordial follicle stage.

Methods We utilised mice with complete postnatal deletion of KIT expression in oocytes via *Gdf9-iCre* and conducted analyses on ovarian follicle development, specific markers, hormone assays, and fertility outcomes.

Findings Our findings reveal contrasting phenotypes compared to previous mouse models with prenatal deletion of *Kit*. Specifically, postnatal deletion of *Kit* exhibit no defects in germ cell nest breakdown, follicle activation, and folliculogenesis during development. Remarkably, upon reaching full maturity, mice with postnatal deletion of *Kit* experience a complete loss of ovarian reserve, growing follicles, and ovarian function. Furthermore, mice display smaller ovarian size and weight, delayed folliculogenesis, and phenotypes indicative of primary ovarian insufficiency (POI), including elevated serum levels of FSH, reduced AMH, and absence of ovarian follicles, ultimately resulting in infertility. Additionally, the ovaries exhibit randomly distributed expression of granulosa and theca cell markers such as Inhibin α, ACVR2B, and LHR. Notably, there is the uncontrolled expression of p-SMAD3 and Ki67 throughout the ovarian sections, along with the widespread presence of luteinised stroma cells and cleaved Caspase-3-positive dying cells.

Interpretation These genetic studies underscore the indispensable role of KIT in oocytes for maintaining the survival of ovarian follicles and ensuring the reproductive lifespan.

Funding This work was supported by National Institutes of Health grant R01HD096042 and startup funds from UNMC (S.Y.K.).

Keywords: KIT; Oocyte; Folliculogenesis; Survival; Primary ovarian insufficiency; Infertility

Introduction

The ovary is an essential organ, not only responsible for producing female germ cells but also for synthesising endocrine hormones crucial for maintaining homeostasis within the female body.[1] Hormones secreted by developing ovarian follicles play a pivotal role in regulating the menstrual cycle and ensuring the overall health of various organs, including the brain, heart, bone, breast, skin, and uterus.[2,3] Comprising oocytes, surrounding granulosa and theca cells, as well as stromal cells, the ovary has different stages of ovarian follicles.[4,5] Among these, the primordial follicle stands as the smallest ovarian follicle, comprising an oocyte surrounded by squamous pregranulosa cells.[6] Serving as the reservoir of ovarian reserve, primordial follicles remain in a dormant state throughout a woman's reproductive lifespan until they undergo activation.[7–9] When primordial follicles are activated, squamous pregranulosa cells undergo transformation into cuboidal granulosa cells, forming multilayers around the oocyte. As follicles progress in development, both oocytes and granulosa cells undergo preparations for ovulation.

*Corresponding author. Olson Centre for Women's Health, Department of Obstetrics and Gynaecology, College of Medicine, University of Nebraska Medical Centre, 985860 Nebraska Medical Centre, Omaha, NE 68198, USA.
E-mail address: soyoun.kim@unmc.edu (S.-Y. Kim).
[c]These authors contributed equally to this work.

Research in context

Evidence before this study

KIT expression begins prenatally in female germ cells, and various lines of evidence suggest its necessity for germ cell survival during foetal migration and postnatal ovarian development. Previous studies have highlighted the importance of KIT in the formation and activation of primordial follicle. However, the specific postnatal role of KIT in oocytes during folliculogenesis has not been thoroughly investigated until now.

Added value of this study

Our study elucidates the significance of postnatal KIT expression in oocytes for various aspects of ovarian follicle development and function. We demonstrate that postnatal KIT is crucial for oocyte survival, normal folliculogenesis, antral follicle formation and growth, as well as ovarian hormonal secretion, surpassing its role in oocyte activation. Additionally, deletion of Kit in ovarian follicles leads to uncontrolled stromal cell growth and the formation of luteinised follicles in postpubertal stages. Consequently, postnatal deletion of Kit results in diminished ovarian follicles, ultimately leading to infertility and a phenotype resembling POI in mice.

Implications of all the available evidence

Evidence suggests a critical role for KIT in oocyte development, survival, and fertility. Further studies are needed to explore KIT signalling pathways in oocyte development and survival, as well as the clinical relevance to POI.

While multiple primordial follicles are recruited during each menstrual cycle, luteinising hormone triggers the ovulation of a single antral follicle.[10]

KIT serve as the receptor for stem cell factor (SCF), also known as KIT ligand (KITL). Its expression is widespread across various cell types, including germ cells, haematopoietic stem cells, haematopoietic progenitor cells, and melanocytes. The KITL-KIT signalling pathway plays multifaceted and pivotal roles in gametogenesis, fertility, haematopoiesis, and melanogenesis.[11] Specifically, KIT is expressed in oocytes, as well as in theca and interstitial cells within the ovary, while KITL is secreted from granulosa cells. This suggests the importance of the KITL-KIT signalling pathway in oocyte growth and follicular development.[12,13] Numerous studies provide evidence supporting the necessity of *Kit* expression for germ cell survival during migration and the early stage of postnatal ovarian development.[14] Furthermore, mRNA levels of *Kit* and *Kitl* dynamically change throughout the oestrous cycle, regulating essential genes required for ovarian development.[14,15] Thus, the KITL-KIT signalling pathway in oocytes plays a crucial role in ovarian follicle activation and development.

Upon binding of KITL to KIT, the receptors undergo homodimerisation and subsequent autophosphorylation at tyrosine residues, leading to an increase in kinase activity. This activation initiates downstream signalling pathways mediated by various enzymes and adaptor molecules. Specifically, KIT triggers the activation of phosphatidylinositol 3-kinase (PI3K), mitogen-activated protein kinase (MAPK), and the Janus kinase/signal transducer and activator of transcription (JAK/STAT) pathways.[16] Numerous studies have demonstrated that KIT orchestrates the activation of the PI3K pathway and its downstream effectors, facilitating oocyte growth and primordial follicle activation.[17–19] PI3K stands out as a pivotal regulator of oocyte survival.[8,9] Recent in vitro investigations have further underscored the significance of KIT-PI3K signalling in regulating germ cell nest breakdown and primordial follicle formation within the mouse ovary.[20] The MAPK pathway contributes to primordial follicle activation through mammalian target of rapamycin complex (mTORC1)-KITL signalling in granulosa cells, downstream of KIT-PI3K activity in oocytes.[21] As such, these downstream signalling cascades play crucial roles in orchestrating proper follicular development, highlighting the indispensable role of KITL-KIT signalling in ovarian function. This notion finds support in a recent study, which demonstrated the vital communication between oocytes and pregranulosa cells via mTORC1-KITL signalling in pregranulosa cells and KIT-PI3K signalling in oocytes.[22]

POI presents as a disorder affecting women under the age of 40, characterised by a decline in ovarian function, oocyte loss, aberrant folliculogenesis, reduced oestradiol levels, and elevated gonadotropins such as follicle-stimulating hormone (FSH) and luteinising hormone (LH).[23] Women with POI commonly experience diminished ovarian hormone production, leading to fertility challenges. Additionally, oestrogen deprivation heightens the risk of osteoporosis, cardiovascular disease, and cognitive dysfunction in affected individuals. The onset of POI results from a premature decline in ovarian follicle numbers, accelerated follicle depletion, or inadequate follicular response to gonadotropins, culminating in compromised fertility and a significant decrease in ovarian hormone production. However, diagnosing POI often comes unexpectedly, with a considerable number of cases remaining idiopathic in origin. The aetiology of POI is multifaceted, involving genetic, autoimmune, toxic, metabolic, infectious, and iatrogenic factors.[24,25] The optimal management approach for POI typically involves hormone replacement therapy, although further evidence from long-term prospective observational studies is still

necessary. Recently, mutations in the KIT gene have been identified in a woman diagnosed with 46, XX spontaneous POI.[26] DNA sequencing analysis of KIT revealed a variant within the intronic sequence downstream of exon 16, suggesting that specific mutations in the human KIT gene may contribute to the development of POI in women.

A previous study demonstrated the expression of KIT at 17.5 days post coitum (dpc) and its significance in primordial follicle formation and activation, utilising a KIT-blocking antibody.[27] Another study suggested the critical role of KIT signalling in the reawakening of primordial follicles through germ cell-specific Kit conditional knockout (cKO) using *Vasa-Cre*.[28] However, Kit conditional knockout using *Vasa-Cre* results in the loss of KIT expression from an embryonic stage onwards, indicating the necessity for an alternative oocyte-specific Cre system to investigate the role of KITL-KIT signalling in oocyte-to-follicle development both prepubertally and during adulthood in vivo. Notably, only an in vitro study utilising an ACK2 inhibitor reported the importance of KIT in antrum formation within growing follicles.[29]

In a previous study,[28] the kinase domain was deleted from Kit at exon 17, resulting in the blocking of internal downstream signalling using $Kit^{L/-}$. This deletion implied that the extracellular and transmembrane domains likely remained intact in oocytes. The present study utilised a *Gdf9-icre* system, where Cre recombinase expression is detected in oocytes within germ cell nests on postnatal day 0 (PD0), enabling a unique and complete oocyte-specific Kit knockout from germ cell nests to antral follicles.[9,30–33] Our investigation revealed that postnatal KIT expression at the primordial follicle stage plays a pivotal role in oocytes, contributing significantly to ovarian follicle survival, normal folliculogenesis, antral follicle formation and growth, as well as ovarian hormonal secretion, surpassing its role in oocyte activation. Furthermore, depletion of KIT in ovarian follicles led to uncontrolled stromal cell growth and the development of luteinised follicles during the postpubertal stage. Consequently, postnatal deletion of Kit resulted in diminished ovarian follicles, infertility, and ultimately, a phenotype resembling POI in mice. This study underscores the critical importance of KITL-KIT signalling in oocytes for maintaining normal ovarian follicles and function after puberty.

Methods

Animals

CD-1®IGS mice (022, Crl:CD1, ICR) were purchased from Charles River Laboratories (Wilmington, MA) and bred to obtain mouse pups on various postnatal days to assess KIT expression. Additionally, C57BL/6 mice (027, C57BL/6NCrl) were purchased from Charles River Laboratories, and 16-month-old female mice were obtained from the C57BL/6 breeding colony. The day of birth was designated as day 0 (PD0). All histological images with DAB staining in Fig. 1 were obtained from the ovaries of CD-1 female mice. The total number of mice involved in this study is approximately 114. The number of mice in each figure are follows: PD1 (n = 4), 1 week (n = 3), and 2 weeks (n = 3) for Fig. 1; PD1 (n = 4 per each genotype), 1 week (n = 3 per each genotype), 2 weeks (n = 3 per each genotype), and 6 weeks (n = 3 per each genotype) for Fig. 2; 20 weeks (n = 4 per each genotype) for Fig. 3; 20 weeks (n = 3 per each genotype) for Fig. 4; 1 week (n = 3 per each genotype), 2 weeks (n = 4 per each genotype), 6 weeks (n = 3 per each genotype), 13 weeks (n = 3 per each genotype), and 20 weeks (n = 4 per each genotype) for Fig. 5; 1 week (n = 3 per each genotype), 2 weeks (n = 3 per each genotype), 6 weeks (n = 3 per each genotype), 13 weeks (n = 3 per each genotype), and 20 weeks (n = 3 per each genotype) for Fig. 6. Each mouse line carrying *Gdf9-icre* (Tg (Gdf9-icre)5092Coo, Strain #: 011062) and a floxed allele for *Kit* (B6.Cg-$Kit^{tm1.1Sraf}$/Mmjax, MMRRC Strain #: 042035-JAX) was of the C57BL/6J strain and acquired from the Jackson Laboratory (Bar Harbor, ME). The $Kit^{tm1.1Sraf}$ strain includes an green fluorescent protein (eGFP)-reporter allele, enabling cre-inducible *Kit* deletion and labelling of the *Kit*-deficient cells with eGFP.[34] Oocyte-specific *Kit* cKO mice were generated by mating homozygous $Kit^{tm1.1Sraf/tm1.1Sraf}$ female mice with *Gdf9-icre+;* $Kit^{tm1.1Sraf/tm1.1Sraf}$ male. To compare the difference between two groups, we set up multiple experimental cages (*Gdf9-icre+;* $Kit^{tm1.1Sraf/tm1.1Sraf}$ *male x* $Kit^{tm1.1Sraf/tm1.1Sraf}$ female) and obtained multiple litters from different females in different cages. Then, female pups (wild-type, WT or conditional knockout, cKO) were selected and compared at each time point. Thus, all pups with WT and cKO genotypes were randomly selected. *Kit* genotyping was performed via PCR analysis using primer A (5'-CCC GGA GCC CAC AAT AGA TTG-3') and primer B (5'-AAC CAG CTG GGG CTC GAA ATT-3').[34] The WT *Kit* allele was genotyped with primer A and primer D (5'-CTG TCC TGG GAA ATT GCT TTA-3'). Recombination by *Gdf9-icre* was confirmed using primer F1 (CCCGGAGCCCA-CAATAGATTG) and primer R3 (GGGGCGGAATTC-GATATCAAG). The insertion of GFP was verified by primer F2 (GGTGCCCATCCTGGTCG) and primer R2 (TGTCGCCCTCGAACTTCAC). *Gdf9-icre-;* $Kit^{tm1.1Sraf/tm1.1Sraf}$ and *Gdf9-icre+;* $Kit^{tm1.1Sraf/tm1.1Sraf}$ were designated as WT and cKO, respectively. Thus, WT mice served as the control group for cKO littermate mice. Knockout of *Kit* in oocytes was further confirmed via immunofluorescence assay using ovarian tissue sections and the anti-KIT antibody. Animals were provided with food and water *ad libitum* and housed in Comparative Medicine facilities (UNMC, Omaha, NE), maintaining constant temperature, humidity, and a photoperiod of 10 (light)/14 (darkness) (protocol number 18-152-12 UNMC).

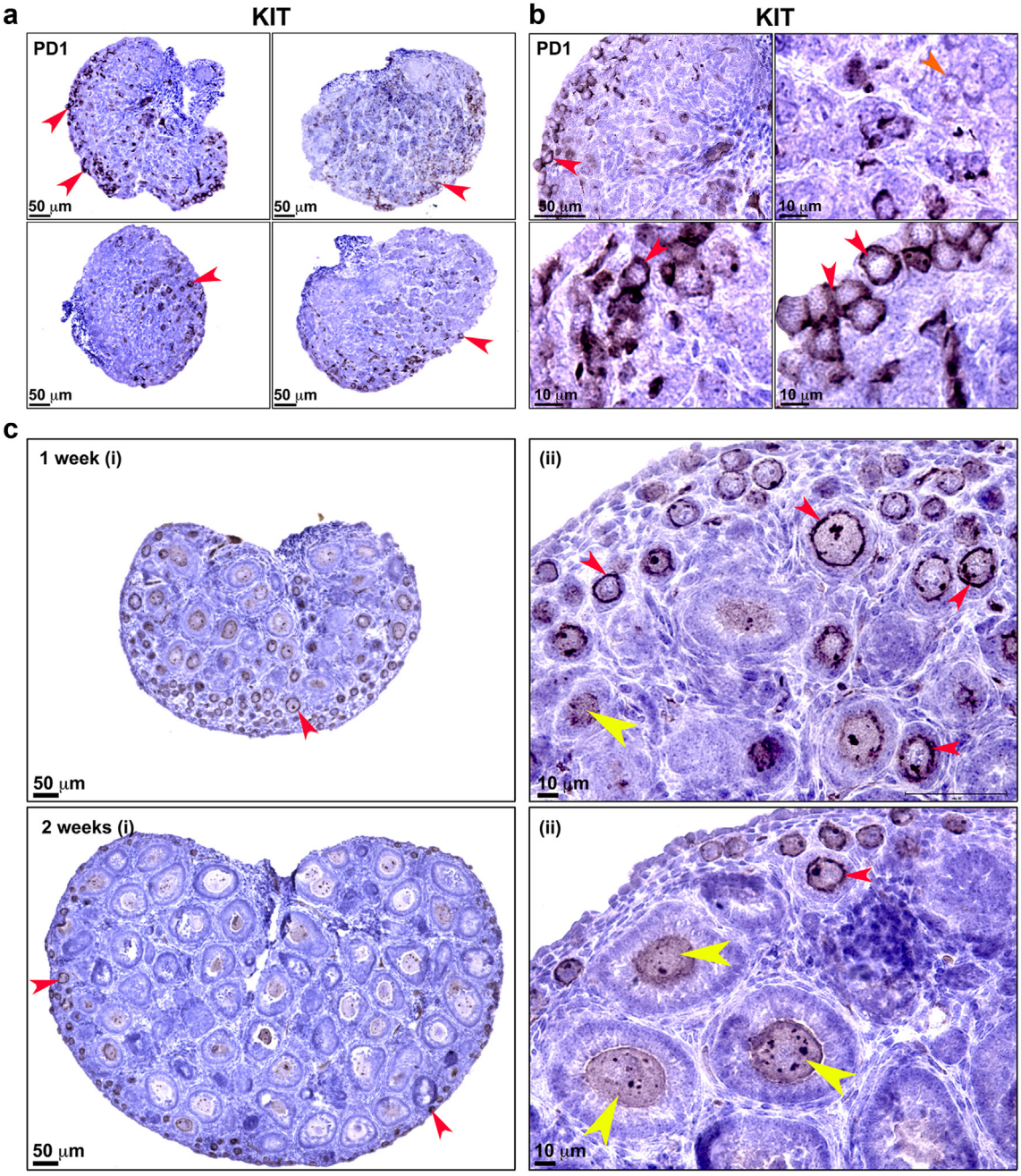

Fig. 1: KIT expression persists from germ cell nest breakdown to early secondary follicle. **(a)** Representative histology and 3, 3-diaminobenzidine (DAB) staining illustrating KIT expression in the ovaries of CD-1 female mice at PD1. Despite all ovaries being obtained from PD1, variations exist in the ovary's shape and germ cell nests distribution. Red arrowheads highlight KIT signals. **(b)** High magnification images of DAB staining in Figure 1a show different levels of KIT expression: red arrowheads indicate very strong KIT expression in germ cell nests, while an orange arrowhead points to germ cell nests with very faint expression. The scale bar in the top left corner is 50 μm; all other scale bars are 10 μm. **(c)** Whole ovarian images from WT mice at 1 week and 2 weeks. Red and yellow arrowheads denote KIT expression in the membrane and cytoplasm of oocytes, respectively. Left: Whole ovarian section image (i); Right: High magnification images of DAB staining showing KIT expression (ii).

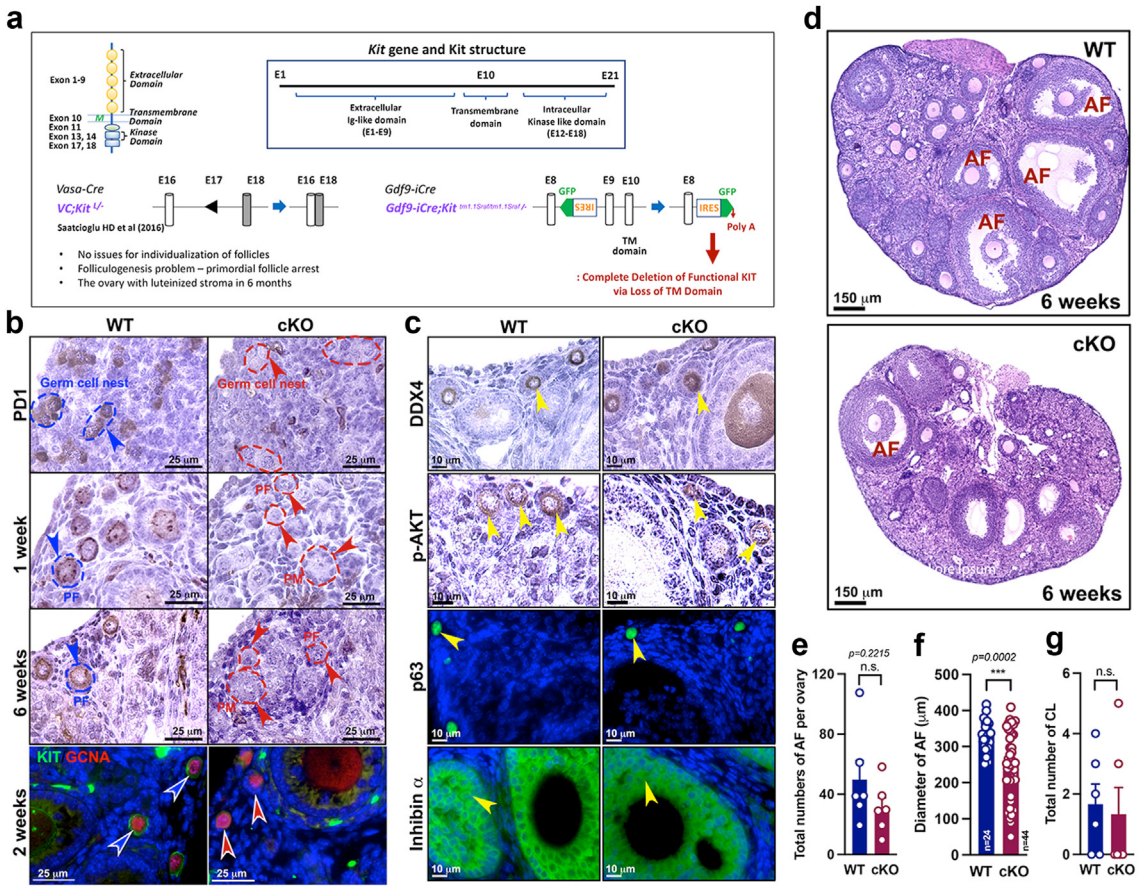

Fig. 2: The absence of *Kit* does not affect early folliculogenesis. **(a)** Schematic illustrating the differences between the *VC;Kit*$^{L/-}$ mouse model and the *Gdf9-iCre+; Kit*$^{tm1.1Sraf/tm1.1Sraf}$ mouse model, both with C57BL/6 strain background. M, Membrane; E, Exon; TM, Transmembrane domain; IRES-GFP-polyadenylation, Internal Ribosome Entry Sites-green fluorescent protein-polyadenylation; eGFP, enhanced green fluorescent protein. Blue arrows indicate the consequences of Cre recombinase. **(b)** Representative DAB staining and immunofluorescence assay with KIT in the ovaries from WT or cKO mice. WT indicates littermates of cKO mice. Blue dotted lines and arrowheads indicate the expression of KIT, while red dotted lines and arrowheads indicate the absenece of KIT expression. A co-immunofluorescence assay was performed using KIT and GCNA1 markers. The expression of KIT is indicated by blue arrowheads, while the absence of KIT is marked by red arrowheads. **(c)** DAB staining with DDX4 and p-AKT, and immunofluorescence assay with p63 and Inhibin α in the ovary at 6 weeks. Oocytes of primordial follicles and granulosa cells are indicated with yellow arrowheads. **(d)** Representative histology of the ovary at 6 weeks. AF, antral follicle. **(e)** Total number of antral follicles per ovary at 6 weeks in WT or cKO mouse ovaries (n = 6/each). *n.s., not significant* **(f)** Diameters of antral follicles (n = 41 for WT and n = 41 for cKO, from n = 5 ovaries for WT and n = 3 ovaries for cKO) were measured. ****, $p < 0.001$ **(g)** Quantification of corpus luteum in WT or cKO mouse ovaries (n = 6/each). *n.s.,* not significant.

Histology, immunofluorescence (IF), and immunohistochemistry (IHC) assays

Ovarian tissues were collected from WT and cKO mice at PD1, 2, 6, 9, 13, and 20 weeks, and fixed in Modified Davidson's Fixative (64133-50, Electron Microscopy Sciences, Hatfield, PA) for no longer than 24 h at 4 °C. Subsequently, tissues were processed, embedded in paraffin, and sectioned at a thickness of 5 μm. Hematoxylin and eosin (H&E) staining were performed using standard methods. Immunofluorescence (IF) and immunohistochemistry (IHC) assays were performed as previously described.[9,30] For IF assays, the ABC-HRP Kit (PK-6100, RRID: AB_2336819, Vector Laboratories, Inc., Newark, CA) and Alexa Fluor 488 Tyramide SuperBoost Kit (B40932, Invitrogen/ThermoFisher Scientific, Waltham, MA) were used, while the Metal Enhanced DAB Substrate Kit (34065, ThermoFisher Scientific) was utilised for DAB staining. The catalogue numbers and dilution of primary antibodies were as follows: KIT (D13A2) (3074S, RRID: AB_1147633, 1:50), p63 (D9L7L) (39692s, RRID: AB_2799159, 1:100), p-AKT (9271S, RRID: AB_329825, 1:50), and p-SMAD3 (9520S, RRID: AB_2193207, 1:50), FOXO3α (D19A7) (12829S, RRID: AB_2636990, 1:100) from Cell Signalling Technology (Danvers, MA); BAX (p-19) (sc-526, RRID: AB_2064668, 1:50), luteinizing hormone receptor (LHR)

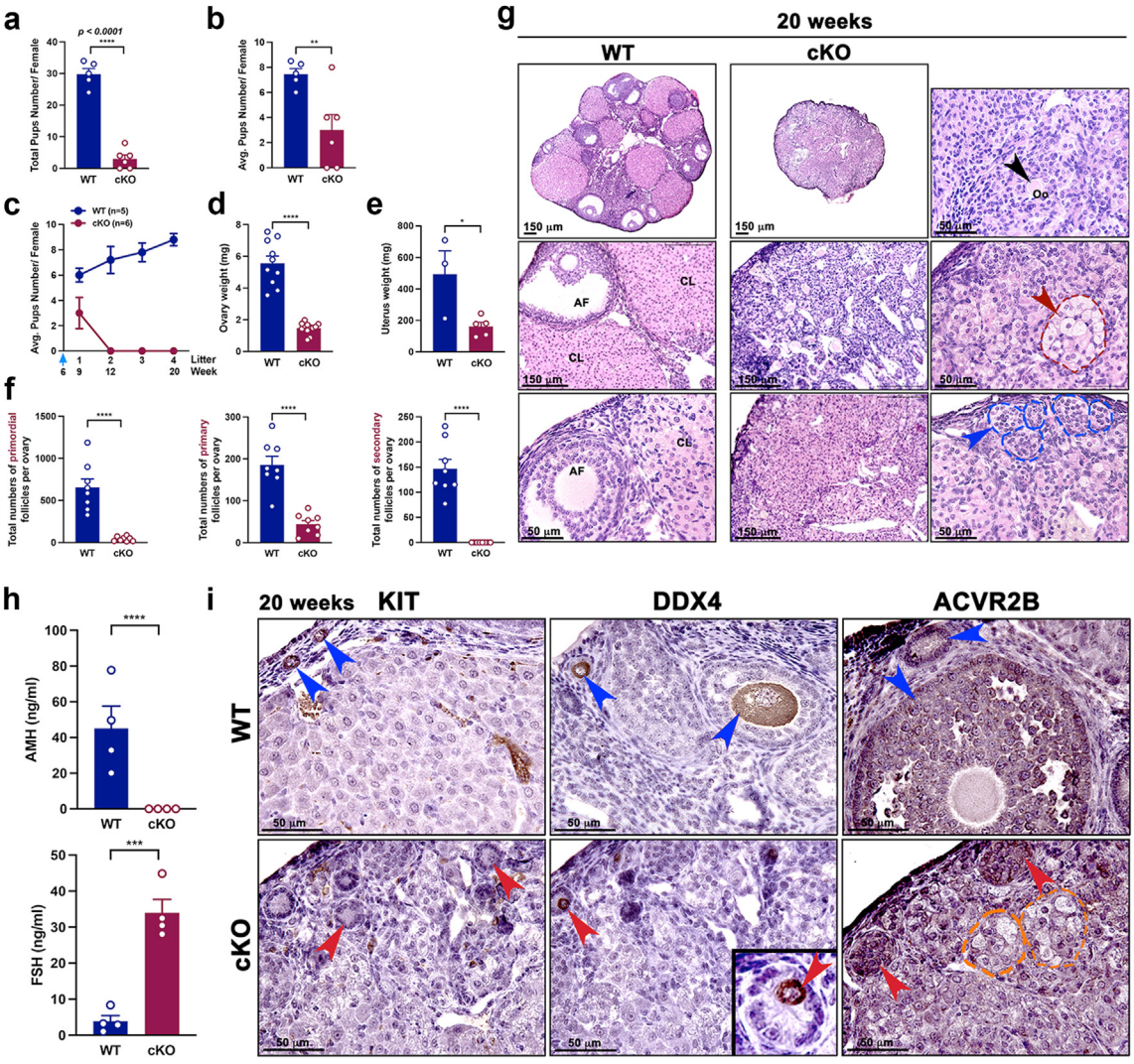

Fig. 3: Loss of *Kit* in oocytes exhibits the phenotype of primary ovarian insufficiency. **(a)** Total number of pups born from females in a mating test. ****, $p < 0.0001$ **(b)** Average number of pups per female resulting from a mating test. **, $p < 0.01$ **(c)** Trend in average number of pups per females over time during the mating test. **(d and e)** Weights of ovaries and uteri post fertility assessment. ****, $p < 0.0001$; *, $p < 0.05$ **(f)** Classification and count of follicles. ****, $p < 0.0001$ **(g)** Histological comparison of WT and cKO ovaries at 20 weeks. Black arrowhead indicates trapped oocyte without granulosa layers. Red arrowhead with red dotted lines shows small clusters of luteal-like cells. Blue arrowhead with blue dotted lines indicates follicle-like structure lacking oocytes. Oo, oocyte; AF, antral follicle; CL, corpus luteum. **(h)** Serum levels of AMH and FSH following fertility tests (n = 4/each group). ****, $p < 0.0001$; ***, $p < 0.001$ **(i)** DAB staining of ovaries from 20-weeks-old females highlighting expression of KIT, DDX4, and ACVR2B. Blue arrowheads indicate positive expression of KIT, DDX4, and ACVR2B in WT ovaries. Red arrowheads indicate the absence of KIT in oocytes of the cKO ovary and point out small and eccentric oocytes in abnormal primary follicle with DDX4-positive oocytes (inset). Additionally, follicle-like structures positive for ACVR2B are designated with red arrowheads. Orange dotted lines outline small clusters of luteal-like cells. Scale bar = 50 μm.

(sc-25828, RRID: AB_2135467, 1:50), and anti-Müllerian hormone (AMH) (sc-6886, RRID: AB_649207, 1:50) from Santa Cruz Biotechnology, Inc. (Dallas, TX); DDX4 (ab270534, 1:100), MSY2 (ab33164, RRID: AB_776541, 1:100), and Ki67 (ab833, RRID: AB_306483, 1:50) from Abcam (Cambridge, United Kingdom); Active (cleaved) Caspase-3 (559565, RRID: AB_397274, 1:50) from BD Biosciences (Franklin Lakes, NJ); Inhibin α (1:100), kindly provided by Dr. Wylie Vale, The Salk Institute (La Jolla, CA); ACVR2B (PA5111122, 1:50) from ThermoFisher Scientific; CD31/PECAM-1 (AF3628, RRID: AB_2161028, 1:100) from R&D systems (Minneapolis, MN); α-Laminin (L9393, RRID: AB_477163, 1:100) from Sigma–Aldrich (St. Louis, MO); GCNA1 (10D9G11, 1:100) from Developmental Studies Hybridoma Bank (DHSB, Iowa

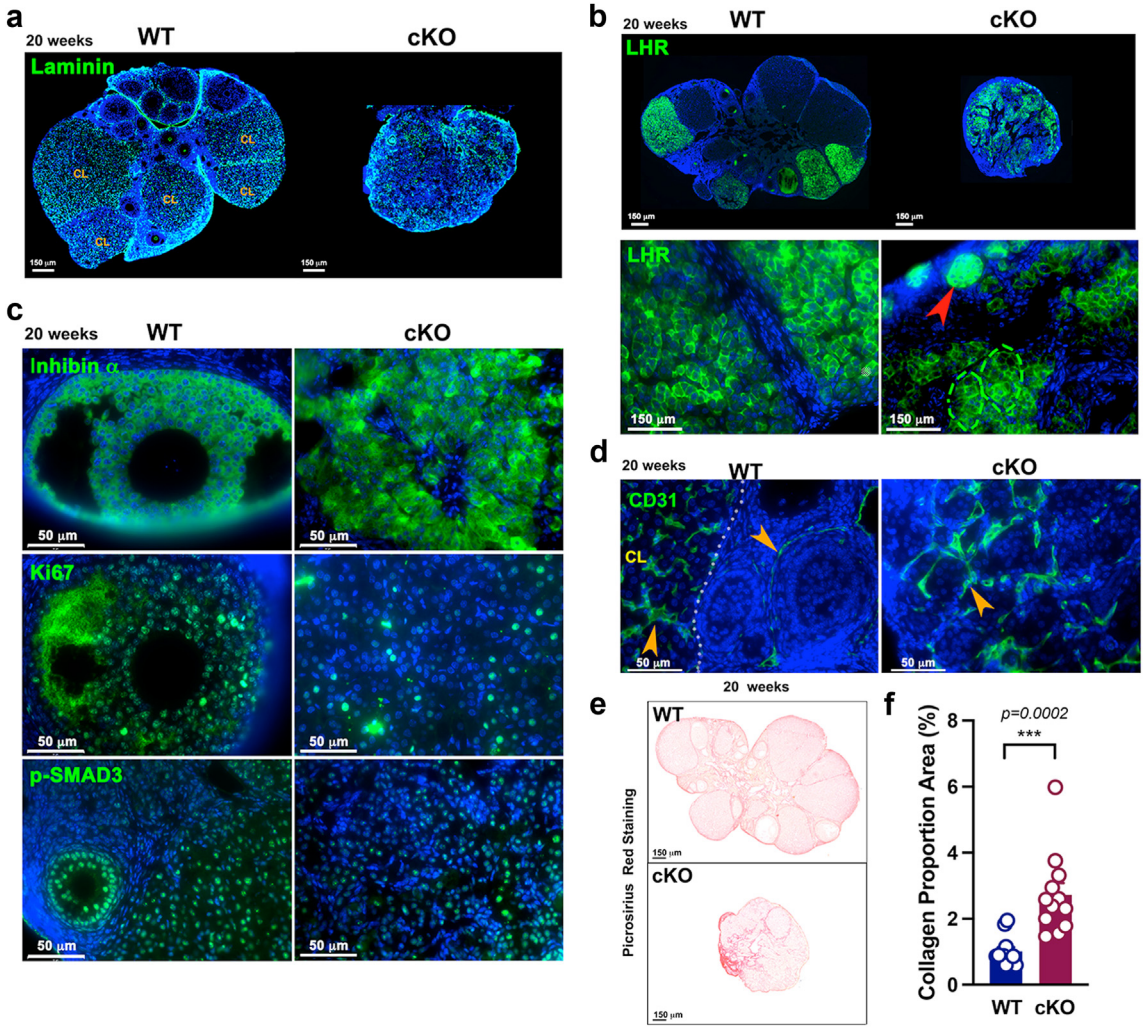

Fig. 4: Mice with oocyte-specific conditional *Kit* knockout exhibit altered expression of ovarian markers. Laminin **(a)**, and luteinizing hormone receptor (LHR) **(b)** were examined using immunofluorescence assays on ovarian sections from 20-week-old females. Red arrowhead indicate follicle-like structures, while green dotted circles highlight small groups of luteal-like cells. **(c)** Inhibin α, Ki67, and p-SMAD3 were evaluated in ovarian sections of WT and cKO mice. Scale bars = 50 μm. **(d)** CD31, a vascular marker, is indicated by orange arrowheads. Scale bars = 50 μm. CL, corpus luteum. **(e)** An image of Picrosirius Red Staining of ovaries from 20-week-old females. Scale bars = 150 μm. **(f)** Collagen proportionate area (CPA%) in WT (n = 3) and cKO (n = 3). ***, $p < 0.001$.

City, IA). Secondary antibodies used were as follows: Goat anti-rabbit IgG (H + L) (BA-1000, RRID: AB_2313606, 1:400) and goat anti-mouse IgG (H + L) (BA-9200, RRID: AB_2336171, 1:400) from Vector Laboratories, Inc.; donkey anti-goat IgG (H + L) (A16003, 1:400) from Invitrogen; Goat anti-rat IgG (H&L) (ab175476, RRID: AB_2813739, 1:200) from Abcam. All primary antibodies were validated with bands of the expected molecular weights and correct localisation of the target proteins. The specificity of secondary antibody binding was confirmed by the absence of signal in negative controls incubated without primary antibodies. All images were captured using the EVOS M7000 Imaging System (AMF700, Invitrogen, Carlsbad, CA).

Follicle counting

Whole paraffin-embedded ovaries were meticulously sectioned at 5 μm thickness using a microtome (Leica RM2125 RTS). Follicle quantification was conducted in every 10th section by three individuals using a randomized approach. The classification and enumeration of ovarian follicle classes followed established protocols.[9] Primordial follicles, characterised by an oocyte enveloped by a single layer of squamous pregranulosa cells, were distinguished. Primary follicles, featuring an oocyte surrounded by a single layer of cuboidal granulosa cells, were similarly identified. In the quantification of primary follicles, primary follicles containing oocytes that are extremely small and eccentrically

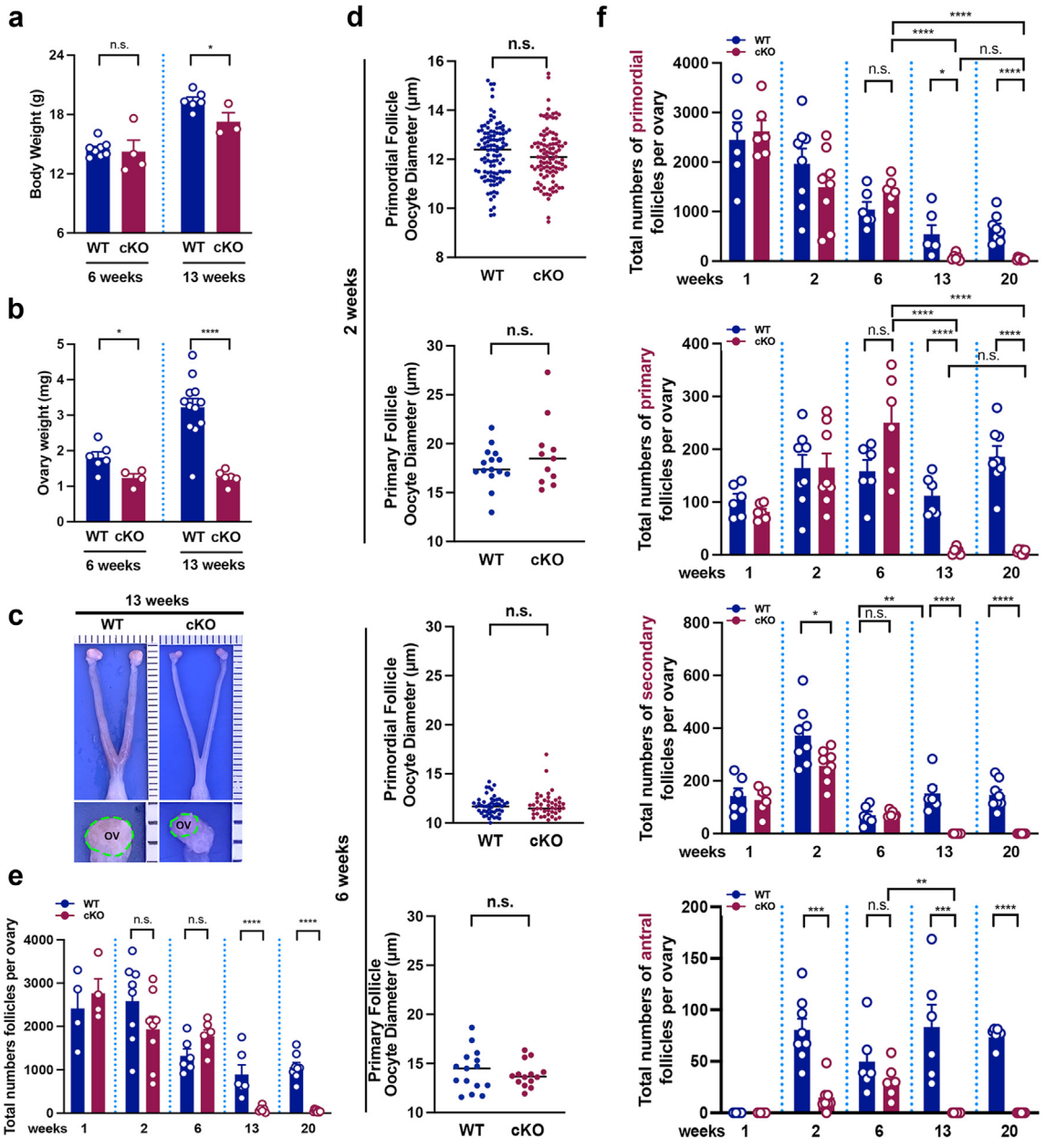

Fig. 5: Kit depletion in oocytes impacts follicle survival but does not block primordial to primary follicle activation. **(a and b)** Body and ovary weight at 6 and 13 weeks. ****, $p < 0.0001$; *, $p < 0.05$; *n.s., not significant* **(c)** Macroscopic images of female reproductive tracts of WT and cKO females at 13 weeks. Green dotted circles depict ovaries attached to oviducts. Ov, ovary. Scale bar in the image represents 1 mm. **(d)** Oocyte diameters were measured at 2 and 6 weeks for both primordial (n = 105 each at 2 weeks and n = 50 at 6 weeks) and primary follicles (n = 15 for WT and n = 11 for cKO at 2 weeks; n = 15 for WT and n = 14 for cKO at 6 weeks), with samples collected from more than three ovaries per group. Statistical significance was noted as follows: *n.s., not significant* **(e)** Total number of follicles per ovary at each time point. ****, $p < 0.0001$; *n.s., not significant* **(f)** Total numbers of each class of follicles at 1, 2, 6, 13, and 20 weeks. One-way ANOVA was used to perform the repeated measures on cKO mice across different weeks. ****, $p < 0.0001$; ***, $p < 0.001$; **, $p < 0.01$; *, $p < 0.05$; *n.s., not significant*.

positioned were included. Secondary follicles, defined by an oocyte encased by multiple layers of cuboidal granulosa cells, and antral follicles, marked by the presence of an antrum of any size, were also discerned. Primordial and primary follicles were tallied only when discernible nuclei were evident within the oocytes, accompanied by healthy pregranulosa cells. Secondary and antral follicles were quantified solely when visible nucleoli were observed within the oocyte nucleus, accompanied by non-atretic and healthy granulosa cells.

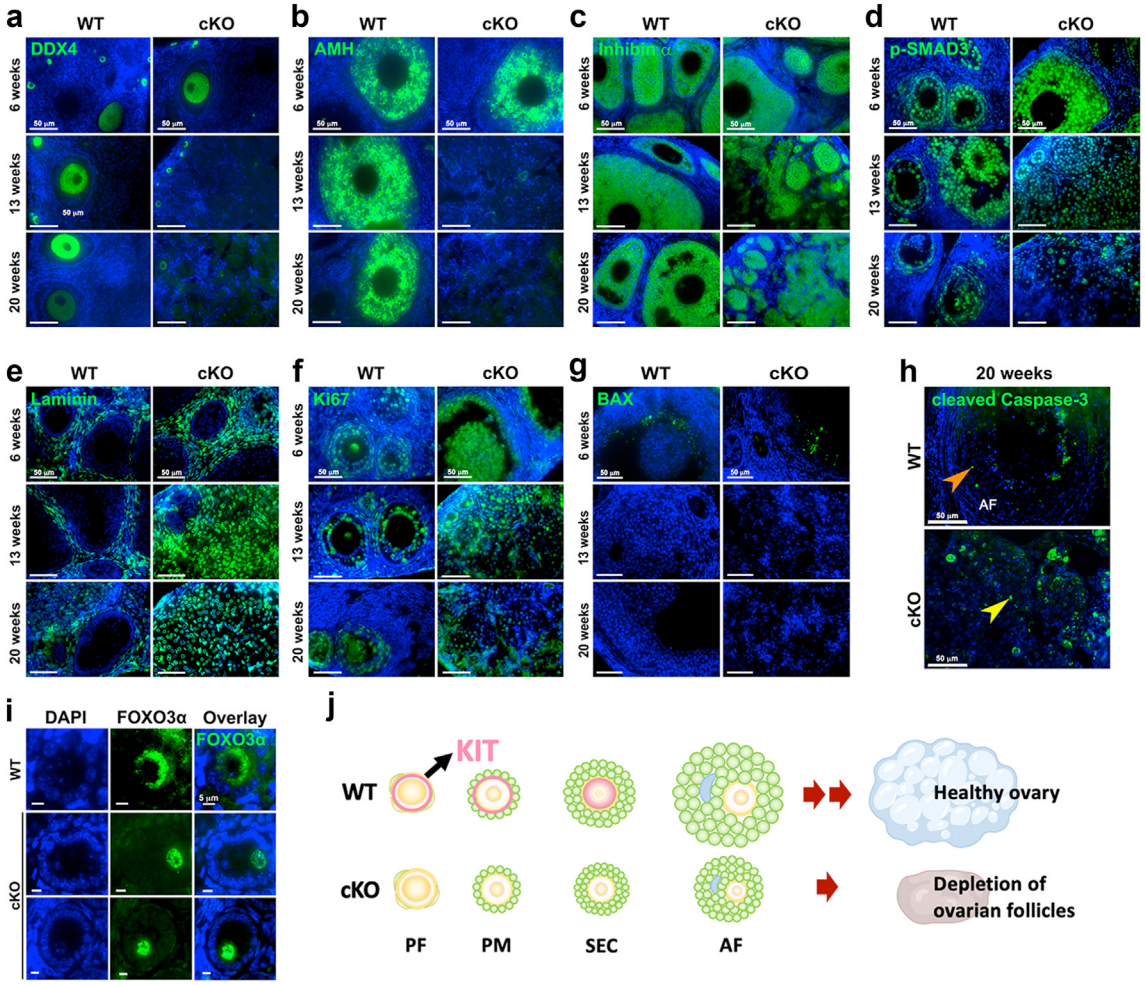

Fig. 6: KIT in oocytes is crucial for oocyte survival and ovarian health. Immunofluorescence assays with ovarian markers in ovarian sections from WT and cKO mice at 6, 13, and 20 weeks. Each protein was visualised with green fluorescence, representing oocyte (DDX4) **(a)**, granulosa cells (AMH, Inhibin α, and p-SMAD3) **(b–d)**, basal lamina cells (Lamanin) **(e)**, proliferation (Ki67) **(f)**, and apoptotic pathway (BAX and cleaved Caspase-3) **(g and h)**. An orange and a yellow arrowheads indicate cleaved Caspase-3 positive cells in WT and cKO, respectively. Scale bar = 50 μm. **(i)** Primary follicles at 6 weeks for WT and at 9 weeks for cKO with FOXO3α. Scale bar = 5 μm. **(j)** Schematic representation of the *Kit* cKO mouse model. PF, primordial follicle; PM, primary follicle; SEC, secondary follicle; AF, antral follicle.

To determine the total count of primordial or primary follicles per ovary, the average follicle count per section was multiplied by the total number of sections and divided by the average count of sections in which a single primordial or primary follicle was observed. The formula used for calculation was (average number of primordial or primary follicles per section × total section number)/2. This division by 2 accounted for the fact that nuclei of primordial and primary follicles spanned an average of two sections due to the approximate 10 μm nucleus span. For total counts of secondary and antral follicles per ovary, the average follicle count per section was multiplied by the total section number. The calculation formula used was (average number of secondary or antral follicles per section × total section number). The WT control group consisted of littermates of cKO mice with a C57BL/6 background.

Diameter measurement for oocytes and antral follicles

The diameters of antral follicles and oocytes in primordial and primary follicles were measured using digital images captured by an EVOS M7000 microscope and analyzed with FIJI software. Antral follicles containing nucleoli were measured, with n = 41 follicles from 5 WT ovaries and n = 41 follicles from 3 cKO ovaries. Antral follicle diameters were measured across the longest length spanning the nucleoli. Oocyte diameters were measured in more than 100 oocytes at 2 weeks and 50 oocytes at 6 weeks for primordial

follicles, and in more than 10 oocytes for primary follicles at both time points, for each genotype (>3 mice per group).

Picrosirius Red Staining

To visualise collagen I and III fibres, ovarian tissue sections (n = 3 each for WT and cKO ovary) were stained using the Picrosirius Red Stain Kit (MER PSR1, Mercedes Scientific, Lakewood Ranch, FL). The staining procedures adhered to the manufacturer's recommended protocol. Ovarian fibrosis was quantified as the Collagen Proportionate Area (CPA), defined as the ratio of the area occupied by PSR-stained collagen fibres to the total area of the section. The analysis was performed at a high magnification of 40x. To test the reproducibility of the quantification, the analysis in Fiji was repeated three times.

Trichrome staining

Masson's Trichrome Stain Kit (25088, Polysciences, Inc., Warrington, PA) was used to evaluate the degree of fibrosis in the organs (n = 3 each for WT and cKO ovary). The procedures adhered to the manufacturer's recommended protocol. Briefly, tissue slides were deparaffinised, mordanted with Bouin's fixative, sequentially stained with Weigert's Iron Hematoxylin Working Solution, Biebrich Scarlet-Acid Fuchsin solution, and Phosphotungstic/phosphomolybdic acid, and Aniline Blue. Finally, slides were mounted with mounting medium.

Serum hormone measurement

Blood samples were collected via cardiac puncture, independent of the oestrous cycle stage. Quantification of FSH and AMH was performed at the University of Virginia Ligand Core Facility. Hormone measurements utilised sera obtained from at least 4 different mice per group.

Fertility test

At PD42, wild-type (n = 5) and *Kit* cKO (n = 6) female mice underwent fertility testing with fertility-proven C57BL/6 males. The reproductive activity of female mice was tracked by recording the total number of litters and pups. The fertility test was concluded when *Kit* cKO females reached 20 weeks of age, at which point their ovaries and uteri were harvested for further analysis. Ovary weights from both ovaries were measured in all females in the fertility test group. Uteri were collected from all six cKO females, while only those from three WT females were collected due to pregnancy at the time of harvest.

Ethics

All procedures (IACUC #18-152-12) involving mice were approved by the Institutional Animal Care and Use Committee (IACUC) at the University of Nebraska Medical Centre (UNMC). The work was conducted in accordance with the ARRIVE guidelines.

Statistics

Graphs were generated using Prism 9.1.1 software (GraphPad Software Version 9, Inc., CA) and are presented as mean with ±S.E.M. We assessed the normality test and homogeneity of variances across all samples. The multiple variable analyses were performed to identify outliers and get descriptive statistics. To directly compare the two groups, independent t-tests with Mann–Whitney test were utilised for evaluating mean differences between the two groups. For comparing more than two groups directly, multiple comparison using repeated ANOVA model with type 3 sums of squares and solution. Regarding the measurement of oocyte diameters, these were measured at 2 and 6 weeks for both primordial and primary follicles, with samples collected from more than 3 ovaries per group. In our study, we determined the effect size drawing upon data from previous research to ensure our study's capacity to identify a statistically significant effect.[9,30,31,35] The sample size of mice in our study was carefully chosen to yield conclusive results, with a significance threshold of 0.05 and a desired power level of 80%. Accordingly, we have included the sample size for each figure in the revised version. p values less than 0.05 were considered statistically significant. n.s. represents not significant, and *, **, ***, and **** represent $p < 0.05$, $p < 0.01$, $p < 0.001$, and $p < 0.0001$, respectively.

Role of funders

The funding sources had no role in the study design, data interpretation, manuscript preparation and final submission.

Results

KIT expression persists from germ cell nest breakdown to early secondary follicle

It has been reported that KIT expression weakly appears in the cytoplasm of mouse oocytes at 16.5 days post coitum (dpc), predominantly on the cell membrane at 18.5 dpc, and exclusively on the cell membrane at postnatal day 1 (PD1).[27] To investigate the expression pattern of KIT in various follicle classes at different developmental stages, we examined KIT expression in the ovaries of CD-1 mice at PD1, 1 week, and 2 weeks postnatally. At PD1, KIT expression was primarily localized to oocytes within germ cell nests in the cortical area (Fig. 1a and b, and Supplementary Fig. S1, red arrowheads). Interestingly, the KIT expression varied both among germline nests and among oocytes within the same nest at PD1 (Fig. 1b and Supplementary Fig. S1). Moreover, sparse KIT expression was detected in oocytes within germ cell nests in the medullary area (Fig. 1b and Supplementary Fig. S1, indicated by

orange arrowheads), while predominant membrane localisation was observed in oocytes in the cortical area at PD1 (Fig. 1b, indicated by red arrowheads). Moreover, KIT expression remained robust in primordial follicles at 2 weeks, indicating its predominant presence throughout ovarian development (Fig. 1c). Additionally, KIT expression persisted during folliculogenesis, with concentrated signals observed on the oocyte membranes of primordial, primary, and early secondary follicles (Fig. 1c, indicated by red arrowheads). Interestingly, KIT expression was detectable in the cytoplasm of oocytes within multilayer secondary follicles in the ovary at 1 and 2 weeks (Fig. 1c i and ii, yellow arrowheads).

The absence of *kit* does not affect early folliculogenesis

To investigate the role of KIT in regulating follicle development, we employed a genetic knockout approach targeting Kit specifically in oocytes, utilizing the *Gdf9-icre* system (Fig. 2a). Previous studies utilised Kit L/- mice, deleting Kit at exon 17 for the kinase domain, suggesting that extracellular and transmembrane domains likely remain in oocytes.[28] However, Kit $^{tm1.1Sraf/tm1.1Sraf}$ mice examined in this study completely removed the KIT receptor from oocyte membranes by deleting exon 9 and onwards, thereby eliminating functional KIT protein via loss of the transmembrane domain 34. A splice acceptor (SA) site followed by internal ribosome entry site (IRES)-GFP-polyadenylation sites was inserted in anti-sense orientation into the intron 8 of the *cKit* upstream from the exon 10, facilitating the complete loss of KIT expression.[34] The oocyte-specific Kit (Kit $^{tm1.1Sraf/tm1.1Sraf}$) cKO mice, generated using the *Gdf9-icre* system (referred to as cKO from hereon) (Supplementary Fig. S2), exhibited an absence of KIT expression in germ cell nests, primordial follicles, primordial follicles (red dotted lines with red arrowheads in Fig. 2b) at PD1, 1 week, 2 weeks, and 6 weeks. In contrast, KIT was highly expressed in the oocytes of wild-type mice (Fig. 2b, blue dotted lines with blue arrowheads). The expression of the *Gdf9* promoter initiated from PD1 in oocytes of germ cell nests and became prominent in oocytes of primordial follicles. Notably, oocytes within germ cell nests transitioned into primordial, primary, and secondary follicles despite the absence of KIT expression (Supplementary Fig. S3a), supported by co-immunofluorescence assay using KIT and GCNA1 antibodies (Fig. 2b). The expression of markers such as DEAD-Box Helicase 4 (DDX4), p-AKT, and p63 for oocytes, as well as Inhibin α and AMH for granulosa cells and Laminin for basal membrane, supported the retention of normal molecular signatures and germ cell identity in oocytes and granulosa cells of 6-week-old *Kit* cKO ovaries when compared to WT ovaries from littermates (Fig. 2c, yellow arrowdeads and Supplementary Fig. S3b). Interestingly, oocytes from *Kit* cKO ovaries consistently exhibited cytoplasmic expression of p-AKT even in the absence of KIT expression (Fig. 2c). Additionally, the number of antral follicles remained comparable between WT and cKO (Fig. 2d and e), while the diameter of antral follicles significantly decreased in 6-week-old *Kit* cKO ovaries [T-test with Mann–Whitney test, $p < 0.0001$] (Fig. 2f). No significant changes were observed in the number of corpus luteum between WT and cKO mice [T-test with Mann–Whitney test, $p = 0.6212$] (Fig. 2g).

The absence of *kit* in oocytes exhibits the phenotype of primary ovarian insufficiency

To assess the reproductive function of oocyte-specific Kit cKO females, a 4-month fertility test was conducted. WT and cKO females were paired with fertility-proven males, and offspring were counted throughout the testing period from 6 weeks (PD42) to 20 weeks (PD140). Results revealed that cKO females exhibited a significant reduction in the total number of pups compared to WT females [T-test with Mann–Whitney test, $p < 0.0001$] and average pups number per female [T-test with Mann–Whitney test, $p = 0.0057$] (Fig. 3a and b). Notably, the ratio of male to female pups remained unaffected in cKO females compared to WT (Supplementary Fig. S4a). While WT females delivered an average of 4 litters over time, cKO females ceased delivering offspring after the first litter (Fig. 3c), implying the subfertility until 9 weeks and became infertile thereafter. Following the fertility test, ovaries from WT and cKO female mice were harvested at 20 weeks for further analysis. The ovarian weight was significantly reduced in cKO females [$p < 0.0001$], along with a decrease in uterine weight compared to WT [T-test with Mann–Whitney test, $p = 0.0261$] (Fig. 3d and e). Additionally, the numbers of primordial, primary, and secondary follicles were all significantly diminished in cKO females compared to WT females [T-test with Mann–Whitney test, $p < 0.0001$] (Fig. 3f). Consistently, the ovaries of cKO females exhibited phenotypic characteristics indicative of complete POI at 20 weeks (Fig. 3g). No growing follicles were observed, though trapped oocytes devoid of follicle structures were noted (black arrowhead). Additionally, the "luteal-like cells", characterised by large oval-shaped cells with nuclei that exhibit reduced eosin staining (red dotted line with red arrowhead in Fig. 3g and green dotted lines in Supplementary Fig. S4b),[28,36,37] is randomly distributed throughout the ovaries of cKO female mice, as indicated by red dotted lines and a red arrowhead. Moreover, "follicle-like structures", which are misshapen round structures with disorganized cells, were observed in the ovaries of cKO mice (blue dotted lines with a blue arrowhead in Fig. 3g and a blue dotted line in Supplementary Fig. S4b). In cKO females, serum AMH levels were undetectable [T-test with Mann–Whitney test, $p < 0.0001$], and serum FSH levels were

significantly elevated compared to WT [T-test with Mann–Whitney test, $p = 0.0003$], indicating ovarian dysfunction in cKO mice (Fig. 3h). To assess the presence of oocytes and granulosa cells in ovarian follicles of 20-week-old cKO ovaries, we performed immunostaining using DDX4, a marker for oocytes, and activin receptor type-2B (ACVR2B),[38] a marker for granulosa cells in growing follicles that exhibit activin A signalling. In WT females, oocytes were clearly visible and stained positive for KIT and DDX4 (Fig. 3i, blue arrowheads), while only a few oocytes within abnormal primary follicle were detected in cKO ovaries (Fig. 3i, red arrowheads). Notably, the abnormal follicles stained with DDX4 contained oocytes that were extremely small and located eccentrically (red arrowheads), consistent with observations in VC; Kit L/- mouse ovaries.[28] In WT ovaries, granulosa cells in growing follicles stained positive for ACVR2B. However, in cKO ovaries, while ACVR2B expression was observed throughout the ovaries, it was predominantly concentrated in 'follicle-like structures' (red arrowheads) (Fig. 3i). Additionally, abnormal structures such as 'luteal-like cells did not exhibit staining for ACVR2B (orange dotted lines in Fig. 3i and pink arrow in Supplementary Fig. S4b).

Molecular signatures indicate abnormal phenotypes in the ovaries of oocyte-specific *kit* conditional knockout mice

To further assess the aberrant characteristics in the ovaries of 20-week-old cKO mice, ovarian markers were examined. Laminin, a major component of the basal lanima,[39,40] typically identifies ovarian follicle structures in a normal ovary. In WT mouse ovaries, laminin-positive cells were primarily localised in basal membrane and the interspace of luteal cells within corpora lutea. However, in cKO ovaries, laminin expression was randomly distributed throughout the ovarian sections (Fig. 4a). The expression of luteinizing hormone receptor (LHR), a marker for theca, mural granulosa, and luteal cells, was typically detected in theca and luteal cells of WT ovaries. However, in cKO ovaries, LHR expression was randomly dispersed within abnormal structures containing luteinizing cells (green dotted lines) and notably elevated in follicle-like structures (red arrowheads in Fig. 4b and a pink arrowhead in Supplementary Fig. S4b). Furthermore, granulosa cell distribution appeared disorganised in cKO ovaries, as evidenced by irregular Inhibin α expression patterns (Fig. 4c). Additionally, markers for proliferation (Ki67) and TGF-β signalling (p-SMAD3) were examined. Ki67- and p-SMAD3-positive proliferating cells were predominantly localised in granulosa cells of WT ovaries, whereas in cKO ovaries, proliferating cells were distributed randomly throughout the tissue (Fig. 4c). CD31, an endothelial cell marker indicated by orange arrowheads, typically appers in the corpus luteum (CL) and the thecal cell layers of growing follicles in WT mouse ovaries; however, in cKO ovaries, its expression is randomly distributed throughout the ovary, as depicted in Fig. 4d. To assess whether the observed phenotypes resembled those of an ageing ovary, known for fibrosis presence, Picrosirius Red staining was used for quantification. The results indicated increased collagen content in cKO ovaries compared to WT ovaries in 20-week-old females (Fig. 4e and f, [T-test with Mann–Whitney test, $p = 0.0002$]). Fibrosis was observed in the ovarian surface epithelial region of cKO mice, as indicated by trichrome staining (Supplementary Fig. S4c), suggesting an ageing phenotype in the ovaries of early-stage cKO female mice.

Severe loss of ovarian follicles occurs post-pubertally in oocyte-specific *kit* conditional knockout mice

To assess the timing of ovarian changes in Kit cKO mice, ovaries were harvested at 6 and 13 weeks. Body weight did not exhibit any significant difference between WT and cKO mice at 6 weeks [T-test with Mann–Whitney test, $p = 0.2398$] but showed a slight decrease in cKO mice at 13 weeks [T-test with Mann–Whitney test, $p = 0.0353$] (Fig. 5a). However, there was a noticeable difference in ovary weight at 6 weeks [T-test with Mann–Whitney test, $p = 0.0282$], which became significantly pronounced by 13 weeks between WT and cKO mice [T-test with Mann–Whitney test, $p < 0.0001$] (Fig. 5b). Visual examination of the female reproductive tract, including the ovaries highlighted with green dots, revealed a marked discrepancy in size at 13 weeks (Fig. 5c).

To investigate the importance of Kit in oocytes during the transition from primordial follicles to primary follicles and to assess its impact on oocyte growth, as previously demonstrated in a study with VC; Kit L/- mice,[28] we measured the diameters of oocytes in primordial and primary follicles at various ages in both WT and cKO ovaries. This approach mirrors the methodology used in the VC; Kit L/- model. Oocyte diameters were similar between WT and cKO mice for primordial and primary follicles at both 2 weeks [T-test with Mann–Whitney test, primordial: $p = 0.3681$, primary: $p = 0.2660$] and 6 weeks [T-test with Mann–Whitney test, primordial: $p = 0.3557$, primary: $p = 0.5483$] as shown in Fig. 5d. These findings indicate that oocytes in cKO mice initially undergo normal development, although they eventually exhibit significant loss of ovarian follicles later.

To assess changes in the numbers of ovarian follicles in Kit cKO ovaries, total follicle numbers were quantified at 1, 2, 6, 13, and 20 weeks. Until 6 weeks, no significant difference in total follicle numbers was observed between WT and cKO ovaries, but a substantial disparity emerged at 13 weeks (Repeated measures ANOVA model, Fig. 5e and Supplementary Fig. S5a). To ascertain which class of follicles was depleted in cKO

ovaries over time, each class of follicles was quantified individually. No significant difference was observed at 1 and 2 weeks between WT and cKO mice, except for the development of secondary and antral follicles (Repeated measures ANOVA model, Fig. 5f and Supplementary Fig. S5b). Notably, the number of primordial follicles in cKO remained comparable to WT at 6 weeks. However, starting from 13 weeks, cKO ovaries exhibited a decrease in the number of all classes of ovarian follicles (Repeated measures ANOVA model, Fig. 5f and Supplementary Fig. S5b). While the number of primordial follicles gradually declined during normal folliculogenesis in WT mice, accompanied by an increase in primary, secondary, and antral follicles, cKO ovaries experienced a dramatic decrease in primordial follicles at 13 and 20 weeks, along with a significant reduction in primary, secondary, and antral follicles (Repeated measures ANOVA model, Fig. 5f and Supplementary Fig. S5b). Notably, all classes of ovarian follicles disappeared between 6 and 13 weeks in Kit cKO females.

KIT in oocytes is crucial for oocyte survival and ovarian health

To investigate the mechanism of follicle loss in Kit cKO ovaries and the impact of ovarian follicle loss, we examined molecular signatures in ovaries from WT and cKO mice between 6 and 20 weeks. The oocyte marker DDX4 was detected in different classes of follicles throughout folliculogenesis, from 6 to 20 weeks, in WT mice. In contrast, cKO ovaries from 13 to 20 weeks contained only DDX4-positive abnormal primary follicles. At 6 weeks, however, they were comparable to WT (Fig. 6a). Furthermore, the expression of anti-Müllerian hormone (AMH), indicative of granulosa cell functionality, was dramatically reduced in cKO ovaries at 13 weeks compared to WT due to the lack of normal growing follicles at 13 weeks (Fig. 6b). Additionally, cKO ovaries exhibited random and patchy expression of Inhibin α in disorganized structures, while WT ovaries presented normal growing follicles with Inhibin α-positive granulosa cells (Fig. 6c). Moreover, p-SMAD3, highly expressed in growing granulosa cells, was ubiquitously expressed in all sections of Kit cKO ovaries, particularly in cells of follicle-like structures at 13 weeks and in unidentified cell types at 20 weeks (Fig. 6d). This suggests that granulosa cells with loss of functionality dispersed throughout the Kit cKO ovary at 20 weeks. Laminin was found to be ubiquitously expressed in cKO ovaries, indicating structural changes in ovarian follicles (Fig. 6e). Unexpectedly, the proliferation marker Ki67 was highly upregulated in the cKO ovary throughout the ovarian sections after 6 weeks compared to the WT ovary (Fig. 6f). Notably, molecular signatures such as Inhibin α, Ki67, and LHR differed between 16-month-old aged females and Kit cKO ovaries (Supplementary Fig. S6). This suggests that the changes observed in advanced-stage Kit cKO ovaries are not related to ageing.

In the Kit cKO ovary, primordial follicles failed to transition to primary or secondary follicles, resulting in depletion across all follicle classes from 6 weeks onwards. To determine if oocytes and granulosa cells underwent apoptosis, we examined BAX, an apoptotic marker. Despite the presence of degenerated structures and dying cells in cKO ovaries, BAX expression was not detectable between 6 and 20 weeks (Fig. 6g). However, cleaved Caspase-3, normally observed predominantly in granulosa cells in the antrum area of antral follicles (indicated by a orange arrowhead), was observed throughout the ovarian sections of 20-week-old cKO ovaries (Fig. 6h, indicated by a yellow arrowhead). This pattern suggests that apoptosis occurred in ovarian cells of cKO ovary.

To investigate the impact of *Kit* loss on the transition from primordial to primary follicles, FOXO3α was analyzed in cKO ovaries. While FOXO3α was predominantly expressed in the cytoplasm of primary follicles in WT ovaries at 6 weeks, its expression remained primarily nuclear even as primordial follicles transitioned to abnormal primary follicles in Kit cKO ovaries at 9 weeks (Fig. 6i). Normally, when oocytes express KIT, folliculogenesis progresses to support a healthy ovary. However, in the absence of KIT protein in oocytes, folliculogenesis and antral follicle growth are delayed, ultimately leading to the loss of ovarian follicle as female mice mature (Fig. 6j and Table 1).

Discussion

The transgenic mouse model featuring oocyte-specific *Kit* cKO used in this study exhibited distinct phenotypes, characterised by normal germ cell nest breakdown, primordial follicle activation, and folliculogenesis until 6 weeks. These observations contrast with those observed in the *VC; Kit*$^{L/-}$ mouse model. However, the role of KIT before germ cell nest breakdown could not be evaluated in this mouse model due to the postnatal expression of *Gdf9-icre*. Notably, the ovaries of mice in this study were depleted of growing follicles and lacked normal ovarian structures later on, indicating the critical importance of KIT in oocytes for follicle survival and the preservation of reproductive functionality.

The physiological differences between this study and the previously reported *VC; Kit*$^{L/-}$ mouse model may primarily stem from variations in the timing of Cre activity. The *Vasa-cre* is activated around embryonic day 15.0 (e15.0) with over 95% efficiency in female germ cells by birth, reaching over 97% efficiency by postnatal day 3 (PD3).[41] In contrast, the *Gdf9-icre* becomes fully active in 3-day-old ovaries but not before 24 h (1-day-old), as demonstrated through β-galactosidase blue staining in *Gdf9-icre; R26R* mice.[42] Therefore, the timing of *Kit* deletion differs between the two mouse models, demonstrating that postnatal deletion of KIT does not impact germ cell nest breakdown or the developmental

Mouse model	CRE	Mutation	KIT	Ovary phenotype	POI		Molecular signature	
					Weeks	Phenotype	p-AKT	FOXO3a
VC; Kit D818V (L)	*Vasa-cre*	D181V amino acid substitution - > Gain-of-function	Cytoplasm oocyte	• Increase of oocyte diameter • Presence of Corpus Luteum • Atretic oocytes	16	• No follicles • Luteinizing stroma • High LH, FSH	Present	Cytoplasm
VC; $Kit^{L/-}$	*Vasa-cre*	Deletion of Exon 17		• A complete failure of oocyte activation • Presence of Cuboidal Granulosa cells surrounding oocyte • Eccentric location of oocytes	12	• No follicles • Luteinizing stroma	Absent	Constitutive nuclear
Gdf9-icre+; $Kit^{tm1.1Sraf/tm1.1Sraf}$	*Gdf9-icre*	Deletion of Exon 9 and on	None	• Normal folliculogenesis until 6 weeks • Presence of Cuboidal Granulosa cells surrounding oocyte • Eccentric location of oocytes in primary follicles	13	• No follicles • Luteinizing stroma • High LH, FSH	Present	Constitutive nuclear

In this table, we outline the differences among three mouse models related to Kit, highlighting aspects such as the timing of Cre activation (*Vasa-cre* on embryonic day 15 (E15); *Gdf9-icre* around postnatal day 3 (PD3)), the specific exons deleted, the expression of KIT post-deletion, the phenotype of each mouse model, the critical time points for POI, and distinct molecular signatures. POI, primary ovarian insufficiency.

Table 1: **Comparison of ovarian phenotypes among three Kit mutant mouse models.**

switch necessary for primordial follicle formation and postnatal folliculogenesis.[27] Therefore, the differences between the two mouse models with Kit gene deletions contribute further to our understanding of the biological role of KIT both prenatally and postnatally. Secondly, another factor to consider is the differences between the Kit transgenes in the two mouse models. In this Kit cKO study, the *Kit* transgene led to the complete deletion of the intracellular domain of KIT, including a membrane-binding domain 28. Our Kit cKO mouse model, confirmed through metal-enhanced 3,3-diaminobenzidine (DAB) staining with Kit antibody, exhibits the complete deletion of KIT in oocytes of cKO mice from PD1 onwards. In contrast, the *VC; $Kit^{L/-}$* mouse model featured the deletion of *Kit* in exon 17, which led to the loss of the kinase domain while retaining the extracellular and membrane-bound domains.

Another Kit mutant mouse model, *VC; $Kit^{D818V\ (L)}$*, featuring a D818V (Asp to Val) amino acid substitution, exhibits constitutive kinase activity even in the absence of ligand, resulting in dominant gain-of-function effects. This mouse model demonstrates a classic, global activation of primordial follicles characterised by enlarged oocytes and altered KIT expression patterns within the cytoplasm. By 16 weeks of age, *VC; $Kit^{D818V\ (L)}$* mice develop POI, presenting morphological abnormalities and follicles devoid of oocytes. This underscores the critical importance of maintaining the balance of KIT protein expression in oocytes for oocyte survival and the longevity of ovarian follicles.

In another study, female mice harbouring a homozygous Kit^{Y719F} mutation in oocytes, along with *Tsc1* null in pregranulosa cells, exhibited a phenotype characterised by arrest at the primary follicle stage compared to female mice with *Tsc1* null only in pregranulosa cells. This underscores the vital role of KIT-PI3K signalling in oocytes for primordial follicle activation.[22] Other studies have also highlighted the critical role of KIT in regulating primordial follicle formation during germ cell nest breakdown and early folliculogenesis, particularly in primordial follicle activation via the PI3K/Akt pathway.[20,27] Ovaries cultured with ACK2, a KIT inhibitor, exhibited reduced germ cell nest breakdown and delayed primordial follicle development,[20] as KITL is believed to promote the formation of the theca cell layer and directly stimulate ovarian stromal cell proliferation.[43] Yoshida et al. proposed that antral follicle development is regulated by the interaction between KIT and KITL. However, KIT expression becomes barely detectable from the stage of multilayer secondary follicles onwards. Moreover, we were unable to investigate the role of KIT in antral follicles due to the presence of unhealthy oocytes in the growing follicles of our cKO mice, which impacted antral follicle development. This observation aligns with the recognised importance of oocyte-derived soluble factors in the development of preovulatory follicles.[29,44] Consequently, further research is needed to elucidate the role of KIT at the antral follicle stage.

Meanwhile, oocytes from our Kit cKO ovary exhibited cytoplasmic p-AKT signals, a known downstream signalling molecule of KIT. This indicates that the PI3K/Akt signalling pathways are not exclusively to KIT. Additionally, signalling pathways through other receptor tyrosine kinases (RTK) may also significantly contribute to primordial follicle activation. This notion is further supported by the observation that homozygous Kit^{Y719F} female mice, harbouring a mutation on the KIT tyrosine residue 719 that impedes KIT binding to the p85 regulatory subunit of PI3K, underwent primordial follicle activation and remained fertile.[19] Notably, this phenotype resembled that of $Kitl^{Sl\text{-}pan}/Kitl^{Sl\text{-}pan}$ ovaries at 3 weeks of age. This collective evidence suggests that KIT signalling may not be indispensable for primordial follicle activation.[19] However, Kit^{Y719F}, $Kitl^{Sl\text{-}pan}/Kitl^{Sl\text{-}pan}$,

and our cKO female mice all exhibited similar phenotypes, characterised by accelerated primordial follicle depletion, accumulation of morphologically abnormal primary/secondary follicles, and arrest at the primary to secondary follicle transition.[19] This implies that while KIT signalling may not be obligatory for primordial follicle activation, it is crucial for maintaining follicle health and lifespan.

The notable phenotypes of Kit cKO mouse models include FOXO3α nuclear localisation in abnormal primary follicles and its persistent presence in luteal-like cells throughout the ovary. A previous study demonstrated that the absence of Kit in oocytes impeded oocyte growth progression and subsequent folliculogenesis. Genetic ablation of Kit within oocytes resulted in primordial follicle arrest in mice, accompanied by constitutive nuclear localization of FOXO3α in oocytes.[28] Upon receiving follicle activation signals, phosphorylated FOXO3α translocates from the nuclei to the cytoplasm of oocytes, facilitating primordial follicle activation and their recruitment into a cohort of primary follicles.[45] In our Kit cKO mouse ovary, FOXO3α expression remained predominantly nuclear in primary and early secondary follicles. Intriguingly, despite the presence of nuclear FOXO3α, primordial follicles progressed into growing follicles without its degradation. The nuclear localisation of FOXO3α in Kit cKO mice suggests that while primordial follicles transition to primary follicles, the oocytes may remain inactive and ultimately fail to mature. A previous study[28] observed a phenotype where ovaries retain numerous luteal-like cells after losing all ovarian follicles, a phenomenon also observed in our Kit cKO mouse ovary. These cells are characterised by their large, round shape and substantial cytoplasm, distinguishing them from other granulosa cells. However, the exact status, role, and fate of these luteal-like cells remain unclear. We hypothesise that the absence of *Kit* in oocytes leads to a slow progression of ovarian follicles before the initiation of the oestrous cycle. However, once the oestrous cycle begins, abnormal primary follicles with compact oocytes fail to proceed with folliculogenesis, leading to the loss of granulosa cells follicles and oocytes. Subsequently, the remaining cells transform into luteal-like cells, eventually contributing to the development of POI phenotypes in the ovary.

Furthermore, the oocyte-specific deletion of *Kit* in both the *VC; Kit*$^{L/-}$ mouse model[28] and the cKO mouse model used in this study led to the development of ovarian POI phenotypes. The cKO mice demonstrated early depletion of ovarian follicles, reduced serum AMH levels–a marker commonly used to assess ovarian reserve and function[46–48]–and elevated serum FSH. These phenotypes in early-stage cKO ovaries mimic an ovarian ageing process, similar to that observed in *Wv* mice,[49,50] and are predictive of menopause in women.[51] Importantly, our transgenic cKO mouse model faithfully recapitulates the natural progression of POI without the systemic effects seen with chemotherapy-induced conditions. The increased FSH levels observed in Kit cKO mice indicate an ovarian origin for amenorrhoea, a key clinical marker for diagnosing POI.[23,52] While hormone replacement therapy is commonly used in clinical settings to manage POI, further research is imperative to evaluate its impacts on systemic conditions among women with POI.

The limitations of this study include the following: First, we were unable to pinpoint the exact timepoint of the abrupt transition in ovarian structure. Second, we were unable to identify the mechanism behind ovarian follicle loss. Third, we were unable to determine why this occurs at the onset of regular oestrous cyclicity, including the downstream molecules of Kit. Nonetheless, the pivotal insight gleaned from this study underscores the essential role of KIT in oocytes within the ovary, crucial for the sustenance and development of follicles. KIT facilitates communication between oocytes and granulosa cells, thereby supporting reproductive longevity. Transgenic mouse studies manipulating Kit expression, either through overexpression (*VC; Kit*$^{D818V(L)}$) or deletion (*VC; Kit*$^{L/-}$ or *Gdf9-icre+; Kit*$^{tm1.1Sraf/tm1.1Sraf}$), consistently exhibited ovarian follicle depletion and onset of POI. While our investigation has not delineated the precise mechanism behind follicle depletion post-puberty in our mouse model, it indicates that our model is well-suited for elucidating the role of KIT in the oocytes by narrowing down the timeframe and exploring molecular signatures. Overall, our findings underscore KIT's indispensability in oocytes, highlighting its role in oocyte survival, facilitating communication with granulosa cells, and maintaining follicular balance within the ovary.

Contributors

YL, WS, and SYK designed the study, performed the experiments, analyzed results, drafted the manuscript, and revised the manuscript. RD and AA revised the manuscript. SYK designed and supervised the study and revised the manuscript. WS and SYK directly accessed and verified the underlying data reported in the manuscript. All authors have read and approved the final version of the manuscript.

Data sharing statement

The data underlying this article will be shared on reasonable request to the corresponding author.

Declaration of interests

The authors declare that they have no conflict of interests.

Acknowledgements

Inhibin α was kindly provided by the late Dr. Wylie Vale at The Salk Institute. FSH and anti-Müllerian hormone (AMH) were measured at the University of Virginia Ligand Core Facility. We thank Dr. Matthew Sandbulte of the Child Health Research Institute at Children's Hospital & Medical Centre and the University of Nebraska Medical Centre for his assistance with manuscript editing. We also extend our gratitude to Dr.

Junghyae Lee of the Department of Biostatistics, College of Public Health, University of Nebraska Medical Center, for her valuable discussions on biostatistics in this study.

Appendix A. Supplementary data

Supplementary data related to this article can be found at https://doi.org/10.1016/j.ebiom.2024.105263.

References

1 Richards JS, Pangas SA. The ovary: basic biology and clinical implications. *J Clin Invest*. 2010;120(4):963–972.
2 Mahboobifard F, Pourgholami MH, Jorjani M, et al. Estrogen as a key regulator of energy homeostasis and metabolic health. *Biomed Pharmacother*. 2022;156:113808.
3 Richards JS, Ascoli M. Endocrine, paracrine, and autocrine signaling pathways that regulate ovulation. *Trends Endocrinol Metab*. 2018;29(5):313–325.
4 Baerwald AR, Adams GP, Pierson RA. Ovarian antral folliculogenesis during the human menstrual cycle: a review. *Hum Reprod Update*. 2012;18(1):73–91.
5 Richards JS, Jahnsen T, Hedin L, et al. Ovarian follicular development: from physiology to molecular biology. *Recent Prog Horm Res*. 1987;43:231–276.
6 Wear HM, McPike MJ, Watanabe KH. From primordial germ cells to primordial follicles: a review and visual representation of early ovarian development in mice. *J Ovarian Res*. 2016;9(1):36.
7 McGee EA, Hsueh AJ. Initial and cyclic recruitment of ovarian follicles. *Endocr Rev*. 2000;21(2):200–214.
8 Kim SY, Kurita T. New insights into the role of phosphoinositide 3-kinase activity in the physiology of immature oocytes: lessons from recent mouse model studies. *Eur Med J Reprod Health*. 2018;3(2):119–125.
9 Kim SY, Ebbert K, Cordeiro MH, et al. Cell autonomous phosphoinositide 3-kinase activation in oocytes disrupts normal ovarian function through promoting survival and overgrowth of ovarian follicles. *Endocrinology*. 2015;156(4):1464–1476.
10 Richards JS. From follicular development and ovulation to ovarian cancers: an unexpected journey. *Vitam Horm*. 2018;107:453–472.
11 Lennartsson J, Rönnstrand L. Stem cell factor receptor/c-Kit: from basic science to clinical implications. *Physiol Rev*. 2012;92(4):1619–1649.
12 Hutt KJ, McLaughlin EA, Holland MK. Kit ligand and c-Kit have diverse roles during mammalian oogenesis and folliculogenesis. *Mol Hum Reprod*. 2006;12(2):61–69.
13 Thomas FH, Ismail RS, Jiang JY, Vanderhyden BC. Kit ligand 2 promotes murine oocyte growth in vitro. *Biol Reprod*. 2008;78(1):167–175.
14 Motro B, Bernstein A. Dynamic changes in ovarian c-kit and Steel expression during the estrous reproductive cycle. *Dev Dyn*. 1993;197(1):69–79.
15 Hutt KJ, McLaughlin EA, Holland MK. KIT/KIT ligand in mammalian oogenesis and folliculogenesis: roles in rabbit and murine ovarian follicle activation and oocyte growth. *Biol Reprod*. 2006;75(3):421–433.
16 Lemmon MA, Schlessinger J. Cell signaling by receptor tyrosine kinases. *Cell*. 2010;141(7):1117–1134.
17 John GB, Gallardo TD, Shirley LJ, Castrillon DH. Foxo 3 is a PI3K-dependent molecular switch controlling the initiation of oocyte growth. *Dev Biol*. 2008;321(1):197–204.
18 Ezzati MM, Baker MD, Saatcioglu HD, et al. Regulation of FOXO3 subcellular localization by Kit ligand in the neonatal mouse ovary. *J Assist Reprod Genet*. 2015;32(12):1741–1747.
19 John GB, Shidler MJ, Besmer P, Castrillon DH. Kit signaling via PI3K promotes ovarian follicle maturation but is dispensable for primordial follicle activation. *Dev Biol*. 2009;331(2):292–299.
20 Burton JJN, Luke AJ, Pepling ME. Regulation of mouse primordial follicle formation by signaling through the PI3K pathwaydagger. *Biol Reprod*. 2022;106(3):515–525.
21 Zhao Y, Zhang Y, Li J, et al. MAPK3/1 participates in the activation of primordial follicles through mTORC1-KITL signaling. *J Cell Physiol*. 2018;233(1):226–237.
22 Zhang H, Risal S, Gorre N, et al. Somatic cells initiate primordial follicle activation and govern the development of dormant oocytes in mice. *Curr Biol*. 2014;24(21):2501–2508.
23 Stuenkel CA, Gompel A. Primary ovarian insufficiency. *N Engl J Med*. 2023;388(2):154–163.
24 Heddar A, Ogur C, Da Costa S, et al. Genetic landscape of a large cohort of Primary Ovarian Insufficiency: new genes and pathways and implications for personalized medicine. *EBioMedicine*. 2022;84:104246.
25 Ishizuka B. Current understanding of the etiology, symptomatology, and treatment options in premature ovarian insufficiency (POI). *Front Endocrinol*. 2021;12:626924.
26 Shibanuma K, Tong ZB, Vanderhoof VH, Vanevski K, Nelson LM. Investigation of KIT gene mutations in women with 46,XX spontaneous premature ovarian failure. *BMC Wom Health*. 2002;2(1):8.
27 Jones RL, Pepling ME. KIT signaling regulates primordial follicle formation in the neonatal mouse ovary. *Dev Biol*. 2013;382(1):186–197.
28 Saatcioglu HD, Cuevas I, Castrillon DH. Control of oocyte reawakening by kit. *PLoS Genet*. 2016;12(8):e1006215.
29 Yoshida H, Takakura N, Kataoka H, Kunisada T, Okamura H, Nishikawa SI. Stepwise requirement of c-kit tyrosine kinase in mouse ovarian follicle development. *Dev Biol*. 1997;184(1):122–137.
30 Kim SY, Cordeiro MH, Serna VA, et al. Rescue of platinum-damaged oocytes from programmed cell death through inactivation of the p53 family signaling network. *Cell Death Differ*. 2013;20(8):987–997.
31 Kim SY, Nair DM, Romero M, et al. Transient inhibition of p53 homologs protects ovarian function from two distinct apoptotic pathways triggered by anticancer therapies. *Cell Death Differ*. 2019;26(3):502–515.
32 Yu SY, Luan Y, Abazarikia A, Dong R, Lee J, Kim SY. Oocyte CTR1 is not essential for cisplatin-induced oocyte death of primordial follicle. *MicroPubl Biol*. 2022;2022. https://doi.org/10.17912/micropub.biology.000632.
33 Luan Y, Yu SY, Abazarikia A, Dong R, Kim SY. TAp63 determines the fate of oocytes against DNA damage. *Sci Adv*. 2022;8(51):eade1846.
34 Kimura Y, Ding B, Imai N, Nolan DJ, Butler JM, Rafii S. c-Kit-mediated functional positioning of stem cells to their niches is essential for maintenance and regeneration of adult hematopoiesis. *PLoS One*. 2011;6(10):e26918.
35 Kim SY, Ebbert K, Cordeiro MH, et al. Constitutive activation of PI3K in oocyte induces ovarian granulosa cell tumors. *Cancer Res*. 2016;76(13):3851–3861.
36 el-Fouly MA, Cook B, Nekola M, Nalbandov AV. Role of the ovum in follicular luteinization. *Endocrinology*. 1970;87(2):286–293.
37 Eppig JJ. Oocyte control of ovarian follicular development and function in mammals. *Reproduction*. 2001;122(6):829–838.
38 Namwanje M, Brown CW. Activins and inhibins: roles in development, physiology, and disease. *Cold Spring Harb Perspect Biol*. 2016;8(7):a021881.
39 Lee VH, Britt JH, Dunbar BS. Localization of laminin proteins during early follicular development in pig and rabbit ovaries. *J Reprod Fertil*. 1996;108(1):115–122.
40 Heeren AM, van Iperen L, Klootwijk DB, et al. Development of the follicular basement membrane during human gametogenesis and early folliculogenesis. *BMC Dev Biol*. 2015;15:4.
41 Gallardo T, Shirley L, John GB, Castrillon DH. Generation of a germ cell-specific mouse transgenic Cre line, Vasa-Cre. *Genesis*. 2007;45(6):413–417.
42 Lan ZJ, Xu X, Cooney AJ. Differential oocyte-specific expression of Cre recombinase activity in GDF-9-iCre, Zp3cre, and Msx2Cre transgenic mice. *Biol Reprod*. 2004;71(5):1469–1474.
43 Parrott JA, Skinner MK. Kit ligand actions on ovarian stromal cells: effects on theca cell recruitment and steroid production. *Mol Reprod Dev*. 2000;55(1):55–64.
44 Eppig JJ, Schultz RM, O'Brien M, Chesnel F. Relationship between the developmental programs controlling nuclear and cytoplasmic maturation of mouse oocytes. *Dev Biol*. 1994;164(1):1–9.
45 Castrillon DH, Miao L, Kollipara R, Horner JW, DePinho RA. Suppression of ovarian follicle activation in mice by the transcription factor Foxo3a. *Science*. 2003;301(5630):215–218.
46 Visser JA, Schipper I, Laven JSE, Themmen APN. Anti-Müllerian hormone: an ovarian reserve marker in primary ovarian insufficiency. *Nat Rev Endocrinol*. 2012;8(6):331–341.

47 Freeman EW, Sammel MD, Lin H, Boorman DW, Gracia CR. Contribution of the rate of change of antimullerian hormone in estimating time to menopause for late reproductive-age women. *Fertil Steril*. 2012;98(5):1254–1259.e1-2.

48 Iwase A, Nakamura T, Osuka S, Takikawa S, Goto M, Kikkawa F. Anti-Mullerian hormone as a marker of ovarian reserve: what have we learned, and what should we know? *Reprod Med Biol*. 2016;15(3):127–136.

49 Smith ER, Yeasky T, Wei JQ, et al. White spotting variant mouse as an experimental model for ovarian aging and menopausal biology. *Menopause*. 2012;19(5):588–596.

50 Murphy ED, Beamer WG. Plasma gonadotropin levels during early stages of ovarian tumorigenesis in mice of the W x -W u genotype. *Cancer Res*. 1973;33(4):721–723.

51 Sowers MR, Zheng H, Jannausch ML, et al. Amount of bone loss in relation to time around the final menstrual period and follicle-stimulating hormone staging of the transmenopause. *J Clin Endocrinol Metab*. 2010;95(5):2155–2162.

52 Stuenkel CA, Gompel A, Davis SR, Pinkerton JV, Lumsden MA, Santen RJ. Approach to the patient with new-onset secondary amenorrhea: is this primary ovarian insufficiency? *J Clin Endocrinol Metab*. 2022;107(3):825–835.